small NANO MICRO

Dip-Pen Nanolithography

DOI: 10.1002/smll.200800949

Multiplexed Lipid Dip-Pen Nanolithography on Subcellular Scales for the Templating of Functional Proteins and Cell Culture**

*Sylwia Sekula, Jeanette Fuchs, Susanne Weg-Remers, Peter Nagel, Stefan Schuppler, Joe Fragala, Nora Theilacker, Matthias Franzreb, Christer Wingren, Peter Ellmark, Carl A. K. Borrebaeck, Chad A. Mirkin, Harald Fuchs, and Steven Lenhert**

***M**olecular patterning processes taking place in biological systems are challenging to study in vivo because of their dynamic behavior, subcellular size, and high degree of complexity. In vitro patterning of biomolecules using nanolithography allows simplification of the processes and detailed study of the dynamic interactions. Parallel dip-pen nanolithography (DPN) is uniquely capable of integrating functional biomolecules on subcellular length scales due to its constructive nature, high resolution, and high throughput. Phospholipids are particularly well suited as inks for DPN since a variety of different functional lipids can be readily patterned in parallel. Here DPN is used to spatially pattern multicomponent micro- and nanostructured supported lipid membranes and multilayers that are fluid and contain various amounts of biotin and/or nitrilotriacetic acid functional groups. The patterns are characterized by fluorescence microscopy and photoemission electron microscopy. Selective adsorption of functionalized or recombinant proteins based on streptavidin or histidine-tag coupling enables the semisynthetic fabrication of model peripheral membrane bound proteins. The biomimetic membrane patterns formed in this way are then used as substrates for cell culture, as demonstrated by the selective adhesion and activation of T-cells.*

Keywords:
- biomimetics
- cell adhesion
- dip-pen nanolithography
- phospholipids
- proteomics

[*] Dr. S. Lenhert, Dr. S. Sekula, Prof. H. Fuchs
Institut für NanoTechnologie
Forschungszentrum Karlsruhe GmbH
76021 Karlsruhe (Germany)
E-mail: steven.lenhert@kit.edu

Dr. S. Lenhert, Prof. H. Fuchs
Physikalisches Institut
Universität Münster
48149 Münster (Germany)

J. Fuchs, Dr. S. Weg-Remers
Institut für Toxikologie und Genetik
Forschungszentrum Karlsruhe GmbH
76021 Karlsruhe (Germany)

Dr. P. Nagel, Dr. S. Schuppler
Institut für Festkörperphysik
Forschungszentrum Karlsruhe GmbH
76021 Karlsruhe (Germany)

J. Fragala
Nanoink Inc.
Campbell, CA 95008 (USA)

N. Theilacker, Dr. M. Franzreb
Institut für Technische Chemie
Forschungszentrum Karlsruhe GmbH
76021 Karlsruhe (Germany)

Dr. C. Wingren, Dr. P. Ellmark, Prof. C. A. K. Borrebaeck
Lund University, Department of Immunotechnology
SE-221 84 Lund (Sweden)

Prof. C. A. Mirkin
Northwestern University
International Institute for Nanotechnology
Department of Chemistry
Evanston, IL 60208 (USA)

Supporting Information is available on the WWW under http://www.small-journal.com or from the author.

1. Introduction

Biological membranes are heterogeneous structures composed primarily of a combination of lipids and proteins. While the lipid component gives the membrane its two-dimensional (2D) structure and fluidity, much of the diverse function of the membrane is made possible by the associated proteins. Not only must both the lipid and protein components be present for a biological membrane to function but complex and dynamic organization of these components on subcellular levels is also required. In particular, partitioning in the cell membrane (e.g., lipid rafts or domains) can range in size from ≈5 nm up to several micrometers and appears to play roles in cell adhesion and signaling through generation of local concentrations of the ligand above threshold levels within these membrane domains.[1,2]

An intensively studied example of such functional patterns forming in cell membranes is the immunological synapse (IS), which forms when a T-cell adheres to an antigen-presenting cell.[3–5] At these cell–cell contact areas, protein partitioning into certain shapes (e.g., bullseye patterns) has been observed and correlated to the dynamics of T-cell activation. It is thought that the lateral patterning in these synapses and the duration of the stimulatory signal play a role in the T-cell's interrogation of the antigen-presenting cell.[6] It is hoped that controlling the IS (e.g., via biomimetic surfaces) will lead to a novel ability to control immune responses.

A vast amount of work has been done in the surface patterning of functional proteins, primarily microarrays for proteomic analysis or diagnostics[7,8] but also for direct screening of drugs,[9] biological sensors,[10,11] and cell culture.[12–14] The fabrication of arrays with smaller structures is desirable for all of these applications due to a lower requirement for sample volume as well as an increased sensitivity of a smaller spot when both sample volume and analyte concentration are limited. For instance, a 1 μL solution containing a typical protein at a concentration of 1 pM only contains enough molecules to completely cover an area of approximately 30 μm^2 (assuming 50 nm^2 $molecule^{-1}$). As is the case with any type of micro- and nanofabrication, quality control and an ability to read out the function of the patterns (e.g., electrically, optically, magnetically, etc.) are increasing challenges, especially as functional structures reach molecular levels.

In the case of cell-culture applications, which require analysis of co-operative patterning and geometric effects on individual cell surfaces, there is an additional size requirement in that more than one functional protein must be patterned together on a scale below the size of a single cell.[13,15] When this is achieved, the cell response to the surfaces can be used as a readout of the biological function of the pattern.[16,17] Photolithography has been used to pattern one functional protein (anti-CD3 ''activation sites'') and the unpatterned regions were then functionalized by a second protein (tethered intercellular adhesion molecule-1: ICAM-1).[15] That work demonstrated the value of spatially separated, subcellular, multicomponent patterns in the study of T-cell activation and provides a clear motivation for the development of more parallel methods of multiplexed protein patterning.[18] In the case of biomimetic surfaces for T-cell culture, it is particularly desirable to have fluid membranes where multiple ligands are free to diffuse within 2D compartments in order to mimic the dynamic surface properties of an antigen-presenting cell. For this reason, promising studies have been carried out involving T-cell culture on micro- and nanopatterned supported lipid membranes.[16]

Dip-pen nanolithography (DPN) is a suitable method for the direct patterning of lipid membrane components[19] and combinatorial libraries of bioactive and inactive structures in general.[20–22] By using the tip of an atomic force microscope as an ultrasharp pen to locally deliver molecular inks to a surface, DPN has the unique potential to combine the resolution of electron-beam lithography with the integration capabilities of ink-jet printing at a throughput on the scale of microcontact printing.[23–28] DPN has been used both for the direct, nanoscale deposition of functional proteins[29–31] as well as for the fabrication of biochemical templates for selective adsorption.[32–38] The latter approach has proven suitable for further applications, for instance, patterning antibodies for highly sensitive and specific diagnostics[32] and immobilization of entire virus particles via metal-affinity interactions for cell-infectivity studies.[33] Fluid phospholipids (e.g., 1,2-dioleoyl-*sn*-glycero-3-phosphocholine (DOPC, $T_m = -16.5\,^{\circ}C$)) are versatile inks for DPN under humidity-controlled conditions and can be used as a carrier ink for the multiplexed and/or massively parallel patterning of functional lipophilic materials, for example, fluorophore-doped lipids.[19] The phospholipid patterns are deposited as multilayers in air (with lateral resolution down to 100 nm). Depending on the substrate surface energy in solution they either remain stable as multilayers under water (partial wetting) or they spread to form supported lipid bilayers (or monolayers on hydrophobic surfaces) of homogeneous thickness (complete wetting).[39–41]

Here we have developed the method of phospholipid-based DPN for the in vitro integration of simplified biomimetic membrane systems consisting of at least two different lipid head groups that selectively bind two different proteins and are spatially separated on subcellular scales. We first use parallel and multiplexed DPN of DOPC mixed with phospholipids containing biotin and nitrilotriacetic acid (NTA) functional groups. Then, two different proteins are selectively bound to the lipid patterns based on biotin-streptavidin and Histidine-tag coupling. This results in fluid, multivalent biomimetic-patterned membrane systems that are suitable model systems to study biological processes, as demonstrated by the adhesion and activation of T-cells. A schematic illustration of the concept and chemical structures are shown in Figure 1.

2. Results and Discussion

2.1. Multiplexed Phospholipid DPN

In order to reproducibly integrate multiple components on subcellular scales by DPN it is preferable to simultaneously deposit the different materials from different tips in a parallel tip array. This is especially true for the integration of a larger number of components (e.g., more than two), as serial

small NANO MICRO

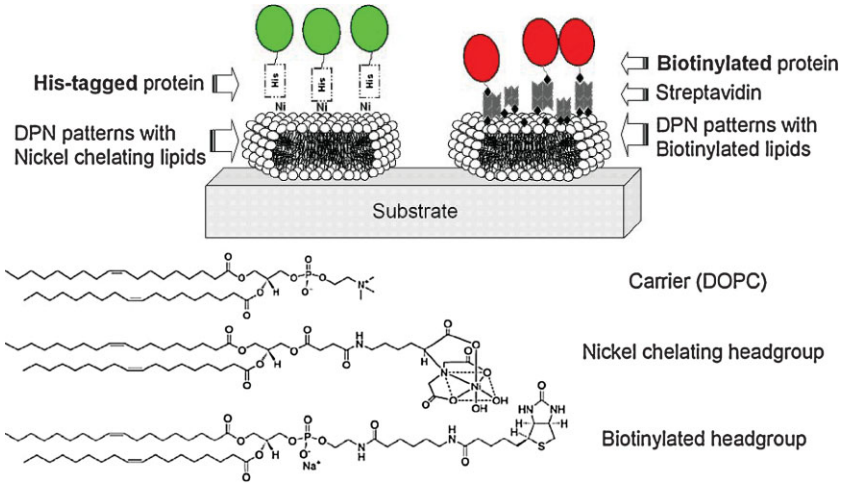

Figure 1. Schematic representation of protein-coupling strategies to spatially patterned lipid supports and chemical structures of the lipids used here.

deposition requires one to exchange the atomic force microscopy (AFM) tip and realign the system between each layer. For this purpose, microfluidic inkwells capable of simultaneously delivering different lipid mixtures to eight different tips in a 26-tip array were used (Figure 2a).[42] In principle, using three of these ink wells would make it possible to integrate 24 different inks onto a single cantilever array. A demonstration of the ability to simultaneously deposit multiple lipid mixtures onto a microscopic area using tips inked in this way is shown in Figure 2b, where each of the 5 different multilayer triangles is composed of a different ratio of the nickel-chelating lipid mixed with DOPC.

Photo-emission electron microscopy (PEEM) is able to provide elemental maps with high resolution and minimum damage to the sample.[43] Since the PEEM data is able to quantitatively monitor both the local carbon signal and the local nickel in the same sample, we use it here to determine whether the ink mixtures prepared maintain their stoichiometric and chemical composition throughout the DPN process. Heterogeneities in the intensity within an individual multilayer pattern in Figure 2b correspond to different local thicknesses of the dehydrated lipid stacks. PEEM imaging indicated that the nickel content in DPN patterns increased linearly with the amount added to the ink up to 25 mol% of the nickel-chelating lipid (Ni-NTA). At higher concentrations of Ni-NTA (e.g., 50%), the ink begins to become less fluid and no longer flows from the tip to the surface at the same rate as at lower concentrations and 100% Ni-NTA did not transfer at all. The triangle corresponding to 50 mol% Ni-NTA in Figure 2b is therefore thinner than the others and shows a lower intensity in the PEEM imaging. The lower-than-expected Ni/C ratios in the PEEM data for 50% Ni-NTA indicate that for ink mixtures prepared at these higher concentrations, the DOPC component begins to transport to the surface at a faster rate than the nickel chelating lipid, comparable to the phase separation observed in mixtures of alkanethiol inks.[44] These data provide confirmation that the phospholipid DOPC functions as an efficient carrier for the Ni-NTA lipids with different head groups at the ratios expected up to 25%. This information is especially important for the planned protein-coupling experiments because more NTA groups are known to increase the binding affinity of the His-tag coupling of proteins to the NTA-nickel lipids.[45]

Perhaps the most unique capability of multiplexed DPN is the ability to integrate different ink materials into complex, combinatorial structural and compositional libraries at high (e.g., subcellular) lateral resolution.[27] This capability is illustrated for phospholipids in Figure 3, where a single cantilever array is used to simultaneously pattern arrays of bullseye-type features of DOPC doped with 1 mol% of rhodamine-labeled and fluorescein-labeled lipids. It has been previously observed that the multilayers are fluid at high humidity (>40%).

When distinct pattern compartments are connected, as in the two multilayer triangle patterns on the top row of Figure 3, it can be seen that the patterns are contiguous and retain their lateral fluidity. Control patterns that are not connected on the bottom row confirm that the mixing takes place on the patterned surface. Since the

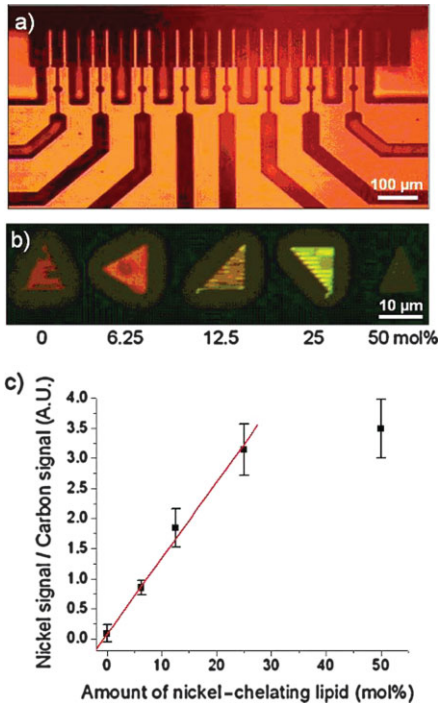

Figure 2. Multiplexed lipid patterning. a) Optical micrograph of a cantilever array (top) approaching microfluidic channels for delivery of up to 8 different inks on the same array. b) PEEM image of patterned multilayers indicating the X-ray absorption that corresponds to the different nickel content of the different multiplexed inks. The image is an overlay of the nickel signal (falsely colored green) and the carbon signal (falsely colored red). Mol% indicates the percent of the nickel chelating lipid mixed with DOPC prior to DPN. c) Plot showing an increasing amount of nickel per carbon measured from the PEEM data shown in b. The amount of nickel in the ink after patterning increases linearly as expected up to 25 mol%. A line is fit to the data up to 25% as an aid to the eye.

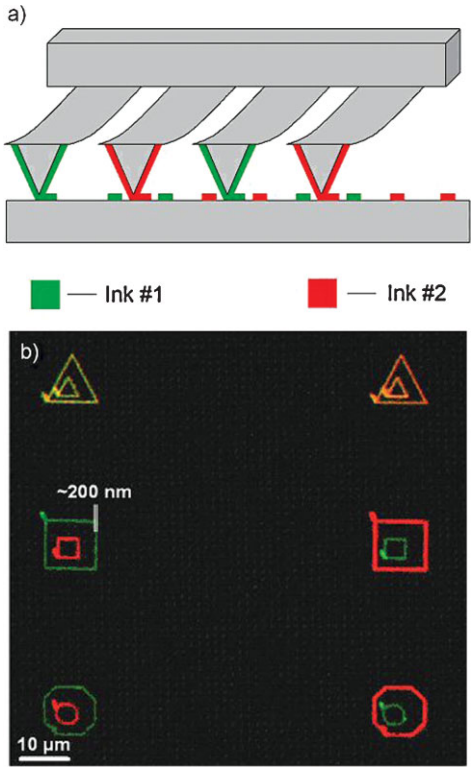

Figure 3. Multiplexed lipid integration for combinatorial nanostructure libraries. a) Schematic illustration of a method used to pattern different lipids on subcellular scales using a single multiplexing DPN cantilever array. b) Multichannel fluorescence images of multilayer structures composed of DOPC doped with two different fluorophore-labeled lipids (rhodamine/red and fluorescein/green) integrated with bullseyes of different shape and topology on subcellular scales. The top two triangle patterns were connected and the two inks mixed to form yellow and orange patterns (depending on the ratios of the red and green pattern volumes), indicating the fluidity of the patterns as well as the possibility of mixing lipids in different amounts using only two different starting inks.

red/green ratios in the fluorescence of the nanostructures correspond to the amount of the ink in each patterned reservoir, this method of mixing lipids on the canvas opens the possibility to create an arbitrary number of mixture combinations on the surface from a limited number of inks on the tips.

The behavior of the DPN-patterned multilayers under water has been previously shown to depend on the substrate.[19] On hydrophilic substrates, the lipids spread to form supported lipid bilayers upon immersion into water (with a loss of some lateral resolution), while on surfaces of intermediate surface energy the nanopatterned multilayers remain stable.[19] For the rest of this work, we therefore use the multilayers for situations where we want to retain lateral resolution and spread monolayers to quantify binding. Since lipid DPN is not dependent on specific substrate chemistry, the ability to deposit multiple different lipid mixtures on subcellular areas could, in principle, be readily combined with existing methods for fabricating diffusion barriers in supported lipid bilayers by DPN writing on pre-patterned substrates.[46]

2.2. Protein Coupling

The selective adsorption of proteins to the functionalized lipid patterns was studied using fluorophore-labeled streptavidin for biotin coupling and His-tagged green fluorescent protein (His-GFP) for metal affinity coupling (Figure 4). The streptavidin/biotin system is widely used because it has one of the largest free energies of association yet observed for non-covalent binding of a protein and small ligands in aqueous solution.[47,48] As the complexes are also extremely stable over a wide range of temperature and pH, the incorporation of biotinylated lipids into lipid monolayers and bilayers is a well-established method for irreversible protein coupling to interfaces and simulating biomembrane processes in vitro.[48–52] His-tag chelator coupling relies on the non-covalent interaction of Histidine residues with a bivalent cation (e.g., Ni^{2+}) that is complexed with an N-nitrilotriacetate (NTA). This coupling method can be reversed by removing the bivalent cations from solution, and the method is therefore widely used in protein purification columns. Chelator lipids have also been developed for incorporation into lipid interfaces and binding of engineered His-tagged proteins.[53–57] Since GFP function is dependent on the conformation of the protein, the fluorescence of His-GFP indicates not only that the protein is present but also that it is in a functional conformation.[58]

In order to determine the optimal amount of the functional lipid to include in the phospholipid ink for protein adsorption, parallel DPN was carried out using biotinylated lipids (1,2-dipalmitoyl-*sn*-glycero-3-phosphoethanolamine-N-(cap biotinyl)) or the nickel-chelating lipid DOGS-NTA-Ni (1,2-dioleoyl-*sn*-glycero-3-{[N(5-amino-1-carboxypentyl)iminodioacetic acid]succinyl} (nickel salt)) mixed with DOPC at various ratios (Figure 4). For the quantitative experiments in Figure 4 (a and b), single lipid bilayer membranes were spread from the DPN multilayers onto hydrophilic glass in order to ensure a homogeneous surface density of binding sites. In both cases, the proteins selectively bound to the functionalized membrane spots upon sufficient blocking with 0.5 weight% of bovine serum albumin (BSA).

In the case of streptavidin (Figure 4a), it was observed that the fluorescence intensity was already saturated at the lowest concentration of the biotinylated lipid used (4.1 mol%; variation in measurements above this percentage are within the experimental error of ≈20%). Although we can not completely rule out the possibility that self-quenching of the Cy3 label on the streptavidin protein may occur at high fluorophore density (e.g., >4 mol%), the data in Figure 4a allow us to conclude that the lipid patterns containing biotin bind the maximum amount of streptavidin detectible by fluorescence microscopy at ≈5 mol% biotin and may already be saturated at lower biotin concentrations. Our measurements are consistent with the literature where strong binding constants[47,48] lead to surface saturation at around 4 mol% based both on calculations of the protein footprint on a lipid bilayer (50 lipids/streptavidin molecule) as well as continuous bleaching measurements.[51] It is known that streptavidin bound to solid supported lipid bilayers at saturating conditions can form crystals[59] and the surface coverage of streptavidin obtained on the spread lipid bilayers used here is expected

NANO MICRO small

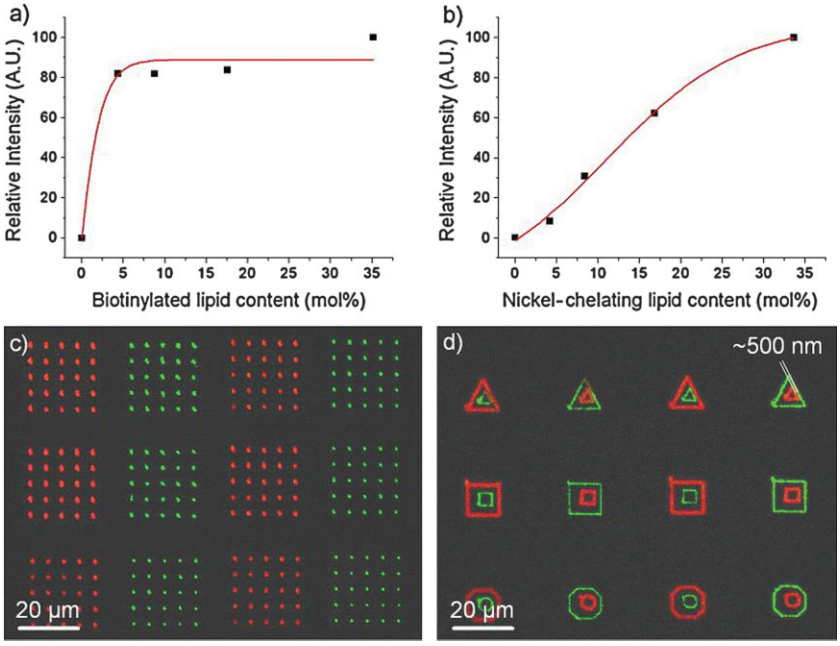

Figure 4. Fluorescence intensity of selectively adsorbed proteins. a) Fluorescence intensity of selectively adsorbed Cy3-streptavidin to spread phospholipid arrays with increasing concentration of biotin head groups. b) Fluorescence intensity of His-GFP selectively adsorbed to spread phospholipid arrays with increasing concentrations of NTA-Ni head groups. Sigmoidal curves are fit to the data. In (a) and (b) phospholipid patterns were deposited on a plasma-treated glass surface and incubated in water to create spread lipid bilayers; (c) and d) are finer, multilayer patterns fabricated on glass used as received, where the lateral resolution is not increased by the bilayer spreading.[19] The image in (d) shows the possibility of integrating two different proteins on subcellular scales. Spot diameters and line widths are measured to be ≈200 nm (the limit of the optical resolution of the fluorescence microscope) and the center-to-center spacing of the two different colored lines is approximately 500 nm.

to be comparable to ≈65% coverage, as measured by ellipsometry and electron microscopy of streptavidin bound to biotinylated lipid Langmuir films.[50,60]

In the case of NTA-Ni, the fluorescence of the bound GFP continued to increase with DOGS-NTA-Ni up to 25% (Figure 4b). This is consistent with the observation that the Histidine binding affinity is additive and therefore a larger amount of nickel on the surface results in stronger binding affinities.[45] These bound proteins appeared unchanged after overnight incubation at 37 °C in phosphate buffered saline (PBS), indicating the irreversibility of the binding. However, upon addition of ethylenediaminetetraacetic acid (EDTA), the proteins immediately desorb, confirming the role of the divalent cations in the binding process (data not shown). Phospholipid inks with NTA concentrations above 25 mol% (i.e., 50% and 100%) were not fluid enough in air (at 75% humidity) to reproducibly flow from the AFM tip during DPN.

Upon determining the optimum ink formulations (5 mol% biotin and 25 mol% NTA), these ink mixtures can then be used for multiplexed DPN to integrate the two different proteins on subcellular scales using multilayer patterns (Figures 4c and d). For this purpose, non-spreading surfaces were used so that the lipids remain as multilayers under water. When the lipid patterns are placed very close to each other, they can occasionally come into contact with the neighbors and mix (e.g., top-left triangles in Figure 4). However, it is possible to place the two different lipid templates with a registry of 500 nm without intermixing of the two different proteins (triangles in Figure 4d). Interestingly, thicker multilayers on surfaces where the lipids do not spread were observed to bind significantly more protein then spread bilayers (data not shown), suggesting that the protein is able to intercalate within multilayers and possibly become encapsulated within the multilamellar stacks.

2.3. Stability in Cell Culture

The phospholipid patterns (without surface-bound proteins) were then exposed to cell-culture conditions in order to determine the stability of the non-covalently bound lipid patterns (Figure 5). Figure 5 shows Jurkat T-cells cultured overnight on a phospholipid mulilayer patterned glass substrate (the ink was DOPC doped with 1 mol% of a fluorescein-labeled lipid). The cells were cultured at a high density of 10^6 cells cm^{-2} in order to ensure cell adhesion (non-specific). Multilayer features with line widths as small as 1 μm appeared unchanged after overnight cell culture, indicating the stability of the non-covalently bound lipid patterns in cell culture (Figure 5b). Spread bilayers were also stable in cell culture (e.g., Figure 6). It is worth noting, however, that use of surfactants or other membrane permeabilizing agents during cell fixation washed away the lipid patterns.

The use of biotin-streptavidin-coupled proteins in cell-culture experiments is well documented.[12,15,61] This coupling method is notoriously stable but tends to result in a relatively random orientation of the protein on the surface. His-tag (or metal affinity)-based coupling is another method for protein immobilization during cell culture.[33,62] His-tag-based binding of proteins to surfaces has the potential advantage that the orientation of the proteins can be controlled to some extent by the genetic engineering of the location of the His-tag on the protein surface.[63] However, in order to use His-tag-based coupling for cell culture, care must be taken to optimize the metal chelating surface such that it retains the His-tagged material in cell-culture conditions.[62] Our study addresses this question by screening different lipid mixtures for their ability to retain fluorophore-labeled His-tagged proteins in cell culture. Figure 6 shows that at high NTA densities (i.e., 25 mol% NTA head groups), His-tagged antibody fragments (red) remain coupled to spread supported lipid membranes (green) during T-cell culture. The darker regions in the centers of the spread lipid membranes in Figure 6a correspond to $10 \times 10\,\mu m$ square multilayer patterns from which the membranes were spread. They are therefore likely due to AFM tip interactions with the substrate. Since the antibody fragments used here (single-chain variable fragment, scFv) can

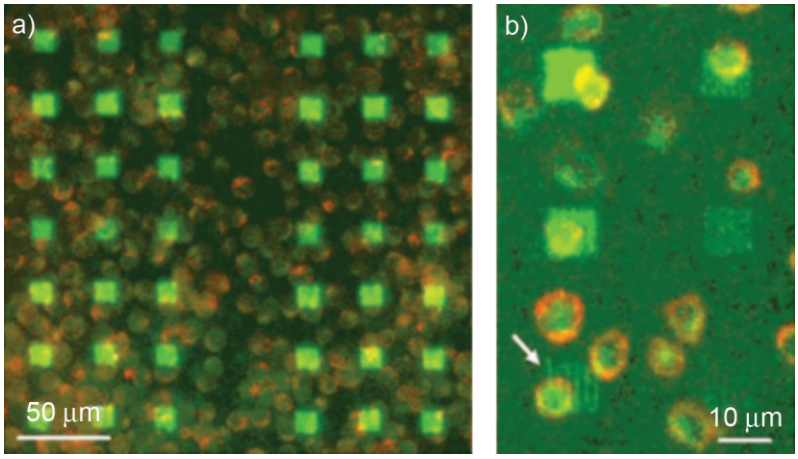

Figure 5. Stability of phospholipid multilayer patterns in cell-culture conditions. Phospholipids were doped with 1 mol% fluorescein-labeled lipids and exposed to a high-density Jurkat T-cell culture in order to ensure cell attachment (non-specific). An overview is shown in (a) and (b) shows a higher magnification. In (b), starting from the top of the image, separation between lines of the nanopattern was varied stepwise: top: 0.5 μm, middle: 1 μm, bottom: 2 μm. The arrow indicates the presence (and therefore stability) of hatch lines with widths below 1 μm (the resolution of the fluorescence characterization is limited in this experiment due to background fluorescence in the cell culture). Micrographs are overlays of fluorescence from the fluorescein-labeled lipids (green) and a dark-field image to identify the cells (falsely colored red).

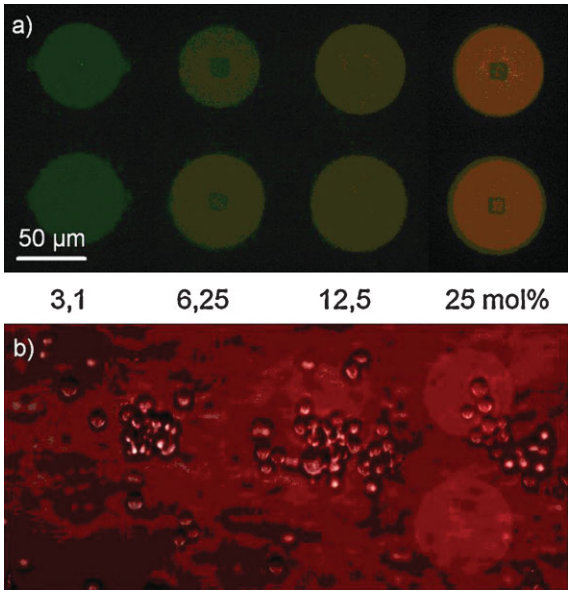

Figure 6. Stability of selectively adsorbed His-tagged proteins to spread lipid membranes in cell-culture conditions. Phospholipid patterns were deposited on a plasma-treated glass surface and spread under water to form supported lipid bilayers. Phospholipids were doped with 3.1, 6.25, 12.5, and 25 mol% NTA-Ni lipids. a) A His-tagged scFv antibody fragment (fluorescently labeled with Alexa 555, shown in red) was coupled to the patterns (doped with 1 mol% fluorescein labeled lipids, shown in green) by NTA-Ni in PBS prior to cell culture. b) Fluorescence image of the protein patterns (red) overlayed with a bright-field image (gray scale) of the cells indicating the stability of the His-tag-based coupling of the antibody fragments in cell culture on lipid membranes with 25 mol% of the NTA-Ni lipids. (a) and (b) are images of the same areas. The red background in (b) is due to autofluorescence of the cell-culture media, which contains phenol red as a pH indicator.

be genetically engineered as libraries,[64] the possibility then exists to carry out functional studies on the co-operative and pattern-dependent function of antibody fragments designed to mimic parts of an antigen presenting cell.

2.4. Protein Function

The vast majority of protein functions rely on a specific molecular conformation of the protein. For instance, the fluorescence function of GFP requires that it be properly folded. GFP is known to unfold at low pH and spontaneously refold upon restoration of higher pH; monitoring the GFP fluorescence at different pH therefore provides an indicator for GFP function.[58] We therefore used GFP fluorescence as an indicator for the function of the membrane bound protein. Fluorescently labeled streptavidin and His-GFP were selectively adsorbed to bivalent multilayer nanopatterns. Next, the nanoarray was treated with pH-3 solution. Under these conditions, loss of GFP fluorescence is observed. Restitution of the pH to level of 9 restores the fluorescence of GFP (Figure 7). The streptavidin fluorescence is not significantly affected under these conditions as the Cy3 dye covalently linked to streptavidin is not sensitive to pH changes in this range.

For the experiment shown in Figure 7, the surface was first blocked with BSA, His-GFP was bound, and then Cy3-streptavidin was bound without a second blocking step. Therefore, some non-specific adsorption of streptavidin is occasionally observable on the GFP patterns, for example, slightly visible in Figure 7c when the GFP fluorescence is inactive. If necessary, the binding specificity could be further optimized by an additional blocking step. It is worth noting that the phospholipids themselves (without bound protein) typically show less non-specific binding than the background (data not shown). While nonspecific binding is an innate disadvantage of the selective adsorption process, when compared with direct write approaches selective adsorption has the advantage that the protein need not be dehydrated and can therefore retain a more native conformation and function.

Finally, as a test of the biomimetic function of the protein-bound lipid patterns and an example of a practical application of lipid DPN nanopatterns in biological studies, we studied the ability of the biomimetic multilayer patterns to activate T-cells. Activating antibodies specific for the CD3 ε chain of the T-cell receptors (α-CD3ε) and and the co-stimulatory receptor (α-CD28) were biotinylated and simultaneously coupled via streptavidin to the biotinylated phospholipid patterns. Jurkat T-cells cultured on these surfaces were observed to selectively adsorb to the corners of square patterns (Figure 8 and Figure S1 of the Supporting Information). Activation of T-cells was observed by examining the expression of the activation marker CD69 using α-CD69-PE detected with α-PETRITC as a read-out (Figure 8a, b, and S2). In control experiments where the functional proteins were replaced by IgG (Figure 8c),

small NANO MICRO

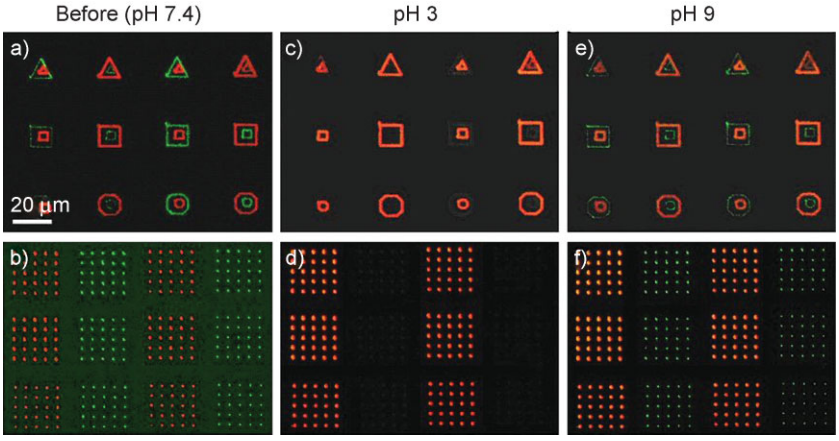

Figure 7. pH-Dependent modification of protein function. Proteins selectively adsorbed to phospholipid multilayer patterns are observed by fluorescence microscopy as a function of pH. The red channel is Cy3-labeled streptavidin while the green channel is GFP. (a) and (b) show proteins adsorbed to nonoarrays under standard conditions; (c) and (d) show nanoarrays in solution at a pH of 3 loose GFP fluorescence; (e) and (f) show them after treatment with a solution of pH 9, leading to restoration of GFP fluorescence. Micrographs in (c–f) were taken with identical optical settings and are shown with the same contrast.

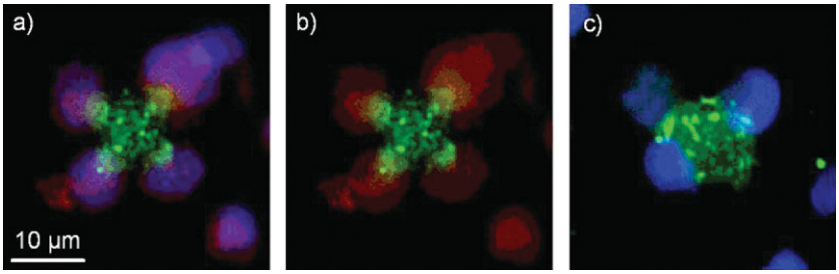

Figure 8. Fluorescence micrographs of T-cells selectively adhered to and activated by functional proteins (anti-CD3/anti-CD28 antibodies) bound to phospholipid multilayer patterns via streptavidin. a) A three-channel image of T-cells adhering to the corners of lipid-protein DPN patterns and activated by anti-CD3/anti-CD28. The green is fluorescence from a fluorescein-doped lipid pattern (10 micrometer square) containing 5% biotinylated lipids. The blue fluorescence indicates the nucleus of the cells by DAPI staining and the red fluorescence shows CD69 expression detected by subsequent staining with α-CD69-PE and α-PE-TRITC. b) A two-channel image showing only the red expression and green DPN patterns from (a). c) A control where the functional proteins were replaced with biotinylated IgG. The cells still adhere to the corners of the patterns but are no longer activated.

significantly less activation was observed, although selective adsorption of the cells to the corners of square patterns still occurred. The selective adsorption to the corners does not appear to be due to the cells preferentially adhering to the glass rather than the lipid patterns (Figures S1 and S2). These results indicate that the selectively bound biotinylated antibodies are able to induce T-cell activation. The observation that cells prefererentially adhere to the corners of the patterns even in the absence of adhesive proteins suggests that they are able to detect a physical signal, for instance, the increased surface energy of curved interfaces.[65,66] As the radius of curvature of the corners of the patterns is <2 μm, this is an example of subcellular features affecting cell behavior.

Another interesting observation from Figure 8 is that the fluorescein dye appears to have formed clusters in the lipid multilayer patterns during this particular experiment. These heterogenieties were not present in the lipid multilayers prior to cell culture and could have several origins, for example, aggregation of the protein, phase separation of the lipids, local changes in the multilayer topography, and so on. More quantitative experiments are necessary to determine the biological significance of these observations and they are mentioned here only as examples of the types of biological experiments that can be carried out using multiplexed lipid DPN. Although we have not yet been able to obtain a suitable combination of His-tagged and biotinylated antibodies to probe the effects of subcellular spatial separation of the different factors, the methods presented here open the door to this possibility.

3. Conclusions

In this study we have presented a method of rapidly fabricating multicomponent, combinatorial, membrane-bound protein patterns based on selective adsorption to phospholipids DPN patterns. DOPC is shown to be a suitable carrier for simultaneous deposition of multiple functional lipids, including biotinylated and nickel chelating lipids mixed in different stoichiometric ratios. These lipids can then be patterned and spatially separated on subcellular scales. The proteins coupled to the lipid patterns retain their function, and the resulting structures are found to be suitable for selective adhesion and activation of T-cells. The methods presented here provide a combinatorial approach to generate functional protein surface patterns that can be used for a variety of biological studies.

4. Experimental Section

Materials: The phospholipids DOPC (1,2-dioleoyl-*sn*-glycero-3-phosphocholine), DOGS-NTA-Ni (1,2-dioleoyl-*sn*-glycero-3-{[N(5-amino-1-carboxypentyl)iminodiacetic acid]succinyl} (nickel salt)), biotinylated phospholipid (1,2-dipalmitoyl-*sn*-glycero-3-phosphoethanolamine-N-(cap Biotinyl) (sodium salt)) and fluorophore-labeled lipids 1,2-dioleoyl-sn-glycero-3-phosphoethanolamine-N-(lissamine rhodamine B sulfonyl) (18:1 lissamine rhodamine/PE) and 1,2-dioleoyl-*sn*-glycero-3-phosphoethanolamine-N-(carboxyfluorescein) were purchased from Avanti Polar Lipids, Alabaster, AL, USA. Cholesterol and chloroform (high-performance liquid chromatography (HPLC) grade) were purchased from Sigma. Nanopure water with a resistivity of 18.2 MΩ cm was used. Glass coverslips (18 mm $\times$18 mm) were purchased from VWR Scientific.

Silicon wafers (native oxide, type N, orientation<111> resistivity 2–5 MΩ cm, purchased from WaferNet Co.) for PEEM measurements were degreased in organic solvents, and then the oxide was removed with 1% HF prior to DPN patterning. Streptavidin (recombinant from Streptomyces avidinii, Cy3 labeled and unlabeled) was purchased from Sigma. α-CD3, α-CD28, and α-CD69-PE antibodies were purchased from BD Pharmingen. α-PE-TRITC antibody was purchased from Rockland (Rockland Immunochemicals). Cell-culture medium and supplements were purchased from Invitrogen Gibco.

DPN patterning: This was performed with commercially available instrumentation (Nscriptor, Nanoink Inc., USA). DPN writing and tip coating were carried out using a commercial DPN writer (Nscriptor, Nanoink Inc, USA) and the following accessories: one-dimensional tip arrays of the D type (A26) and inkwells of type W4 and IWL-0021-01 (NanoInk Inc., USA). The inkwells were filled with a chloroform solution of the phospholipid ink (1 μL, 10 mM, doped with 1 mol% of the dye-labeled lipid in the case of doped inks). The solvent was allowed to evaporate for at least 1 h before coating the tips. Tips were inked by placing them in contact with the inkwell and increasing the humidity to 75% for at least 30 min. Excess ink was removed from freshly coated tips by writing at high humidity (>65%) on a sacrificial substrate for ≈10 min. For preparation of spread lipid bilayers (Figures 4 and 6) glass substrates were plasma treated with oxygen (20 sccm, 100 mTorr, 30 s). Oxygen plasma treatment decreases the contact angle of water, making the substrate more hydrophilic. Membranes were spread by adding water to the dehydrated lipid stacks.

Fluorescence microscopy: This was carried out on an inverted TE 2000 fluorescence microscope (Nikon) and Axioskop 200M deconvolution microscope (Carl Zeiss). Patterns were aligned for imaging using alignment markers scratched onto the glass surface. Bleaching of fluorophores was minimized (especially for quantitative measurements) by first focusing on the alignment mark before exposing the patterned area to light, and the lamp intensity was kept at a minimum. For quantitative measurements of protein adsorption such as that shown in Figure 4, the fluorescence intensity of the different spots was measured using ImageJ.

PEEM: Experiments were carried out at IFP's soft X-ray beamline WERA (WEichRoentgen-Analytik-Anlage) at the ANKA (ANgstroemquelle KArlsruhe) synchrotron light source (Karlsruhe, Germany) in ultrahigh vacuum ($\approx 5 \times 10^{-10}$ mbar) and at room temperature. Photon energies around the C 1s absorption edge at 290 eV and the Ni $2p_{3/2}$ absorption edge at 853 eV were used. The photoexcited and secondary electrons, whose intensity distribution is proportional to the local X-ray absorption of the sample, were imaged using PEEM (Focus GmbH) with an ultimate lateral resolution of about 100 nm. The probing depth of this electron-yield detection mode is in the 5-nm range. For each absorption edge, stacks of typically 100 images for closely spaced photon energies around that edge were recorded, allowing us to extract laterally resolved X-ray absorption spectra and to quantitatively determine the local Ni and C signals depicted in Figures 2b and c.

Cloning and purification of proteins: The GFP derivative used here has a His_6-tag located at the N terminus. The respective gene was transferred into the vector pJOE 4056.2 and cultivated within E. coli (BW3110). After cell harvest the cells were disrupted and the GFP was directly purified from the unclarified homogenate using magnetic microbeads with metal-affinity ligands (iminodiacetic groups loaded with Cu2+) supplied by the company Chemagen (Baesweiler, Germany). The loaded microbeads were washed with PBS and eluted with PBS, 0.5 M imidazol. Finally, the imidazol was removed by the multiple use of centrifugal filter units (Millipore, Amicon Ultra-15, 5 kDa). A human recombinant His-tagged scFv antibody fragment (C1q-4) was stringently selected from the n-CoDeR library[64] and kindly provided by BioInvent International, Lund, Sweden. The high on-chip functionality of deposited scFv antibodies has been extensively demonstrated in the conventional antibody microarray format.[67,68] The scFv antibody was expressed in *E. coli*, purified by affinity chromatography on Ni-NTA agarose (Qiagen, Hilden, Germany), and labeled with Alexa 555 Succinimidyl Ester (Invitrogen, Carlsbad, CA, USA) at a labeling reagent:protein molar ratio of 20:1.

Protein coupling: Patterns prepared on the glass surface were incubated with 0.5% BSA solution in PBS to block unspecific protein binding. The proteins were coupled to the lipid patterns by incubation for 30 min to 1 hour at room temperature in PBS solutions of the His-tagged, streptavidin and/or biotinylated proteins, at protein concentrations ranging from 1–1000 μg mL^{-1}. Samples were thoroughly washed with PBS prior to further processing such as fluorescence microscopy or cell culture. Solutions were exchanged by pipetting into home-made wells cut from thin films of cured poly(dimethysiloxane) (PDMS; Sylgard 184, Dow Corning) placed onto the patterned glass coverslips.

Cell culture: Jurkat T-cells (human T-Lymphoma cell line, purchased from ECACC, UK) were cultured in RPMI1640 medium supplemented with 10% fetal calf serum, 2 mM glutamine, 100 U mL^{-1} Penicillin, 100 μg mL^{-1} streptomycin under standard cell-culture conditions: 37 °C, 5% CO_2/95% air environment. For stimulation of Jurkat cells, streptavidin was bound to biotinylated patterns as described and the surfaces were also incubated with poly-L-Lysin for 10 min prior to binding of biotinylated α-CD3/α-CD28 antibodies or IgG controls. Next 10^6 cells in 400 μL of medium were applied onto samples. Cells were stimulated for 3 h and then fixed in 100 μL od 5% paraformaldehyde solution for 10 min. Cells were washed with PBS and stained with α-CD69-PE (1:10 dilution in PBS) and detected with α-PE-TRITC (30 min, 1:10 dilution in PBS).

Acknowledgements

S.Sekula and S.L. thank the DFG Center for Functional Nanomaterials (CFN E3.2). H.F., S.L., and C.A.M. acknowledge the NSF and DFG. C.A.M also acknowledges the AFOSR for support. The study was in part (C.A.K.B.) supported by the Foundation for Strategic Research (SSF). The ANKA synchrotron is acknowledged for provision of beam time. The PEEM was provided by Focus GmbH through their co-operation with IFP.

[1] A. D. Douglass, R. D. Vale, *Cell* **2005**, *121*, 937.
[2] M. Zeyda, T. M. Stulnig, *Prog Lipid Res* **2006**, *45*, 187.

[3] P. A. Gonzalez, L. J. Carreno, C. A. Figueroa, A. M. Kalergis, *Cytokine Growth Factor Rev.* **2007**, *18*, 19.
[4] A. Grakoui, S. K. Bromley, C. Sumen, M. M. Davis, A. S. Shaw, P. M. Allen, M. L. Dustin, *Science* **1999**, *285*, 221.
[5] C. R. F. Monks, B. A. Freiberg, H. Kupfer, N. Sciaky, A. Kupfer, *Nature* **1998**, *395*, 82.
[6] G. Lezzi, K. Karjalainen, A. Lanzavecchia, *Immunity* **1998**, *8*, 89.
[7] E. Phizicky, P. I. H. Bastiaens, H. Zhu, M. Snyder, S. Fields, *Nature* **2003**, *422*, 208.
[8] C. Wingren, C. A. K. Borrebaeck, *Drug Discov. Today* **2007**, *12*, 813.
[9] Y. L. Hong, B. L. Webb, H. Su, E. J. Mozdy, Y. Fang, Q. Wu, L. Liu, J. Beck, A. M. Ferrie, S. Raghavan, J. Mauro, A. Carre, D. Mueller, F. Lai, B. Rasnow, M. Johnson, H. S. Min, J. Salon, J. Lahiri, *J. Am. Chem. Soc.* **2005**, *127*, 15350.
[10] F. Patolsky, G. F. Zheng, C. M. Lieber, *Anal. Chem.* **2006**, *78*, 4260.
[11] M. P. Jonsson, P. Jonsson, A. B. Dahlin, F. Höök, *Nano Lett.* **2007**, *7*, 3462.
[12] M. R. Hynd, J. P. Frampton, N. Dowell-Mesfin, J. N. Turner, W. Shain, *J. Neurosci. Meth.* **2007**, *162*, 255.
[13] M. Arnold, E. A. Cavalcanti-Adam, R. Glass, J. Blummel, W. Eck, M. Kantlehner, H. Kessler, J. P. Spatz, *ChemPhysChem* **2004**, *5*, 383.
[14] D. Falconnet, G. Csucs, H. M. Grandin, M. Textor, *Biomaterials* **2006**, *27*, 3044.
[15] J. Doh, D. J. Irvine, *Proc. Natl. Acad. Sci. USA* **2006**, *103*, 5700.
[16] K. D. Mossman, G. Campi, J. T. Groves, M. L. Dustin, *Science* **2005**, *310*, 1191.
[17] J. T. Groves, *Curr. Opin. Chem. Biol.* **2006**, *10*, 544.
[18] D. J. Irvine, J. Doh, B. Huang, *Curr. Opin. Immunol.* **2007**, *19*, 463.
[19] S. Lenhert, P. Sun, Y. H. Wang, H. Fuchs, C. A. Mirkin, *Small* **2007**, *3*, 71.
[20] L. M. Demers, C. A. Mirkin, *Angew. Chem. Int. Ed.* **2001**, *40*, 3069.
[21] H. Zhang, S. W. Chung, C. A. Mirkin, *Nano Lett.* **2003**, *3*, 43.
[22] D. A. Weinberger, S. G. Hong, C. A. Mirkin, B. W. Wessels, T. B. Higgins, *Adv. Mater.* **2000**, *12*, 1600.
[23] K. Salaita, Y. H. Wang, J. Fragala, R. A. Vega, C. Liu, C. A. Mirkin, *Angew. Chem. Int. Ed.* **2006**, *45*, 7220.
[24] R. D. Piner, J. Zhu, F. Xu, S. H. Hong, C. A. Mirkin, *Science* **1999**, *283*, 661.
[25] D. S. Ginger, H. Zhang, C. A. Mirkin, *Angew. Chem. Int. Ed.* **2004**, *43*, 30.
[26] K. Salaita, Y. H. Wang, C. A. Mirkin, *Nat. Nanotechnol.* **2007**, *2*, 145.
[27] A. Ivanisevic, K. V. McCumber, C. A. Mirkin, *J. Am. Chem. Soc.* **2002**, *124*, 11997.
[28] Y. Wang, L. R. Giam, M. Park, S. Lenhert, H. Fuchs, C. A. Mirkin, *Small* **2008**, DOI: 10.1002/smll200800770.
[29] K. B. Lee, J. H. Lim, C. A. Mirkin, *J. Am. Chem. Soc.* **2003**, *125*, 5588.
[30] G. Agarwal, R. R. Naik, M. O. Stone, *J. Am. Chem. Soc.* **2003**, *125*, 7408.
[31] D. L. Wilson, R. Martin, S. Hong, M. Cronin-Golomb, C. A. Mirkin, D. L. Kaplan, *Proc. Natl. Acad. Sci. USA* **2001**, *98*, 13660.
[32] K. B. Lee, E. Y. Kim, C. A. Mirkin, S. M. Wolinsky, *Nano Lett.* **2004**, *4*, 1869.
[33] R. A. Vega, C. K. F. Shen, D. Maspoch, J. G. Robach, R. A. Lamb, C. A. Mirkin, *Small* **2007**, *3*, 1482.
[34] R. Valiokas, A. Vaitekonis, G. Klenkar, G. Trinkunas, B. Liedberg, *Langmuir* **2006**, *22*, 3456.
[35] K. B. Lee, S. J. Park, C. A. Mirkin, J. C. Smith, M. Mrksich, *Science* **2002**, *295*, 1702.
[36] M. Lee, D. K. Kang, H. K. Yang, K. H. Park, S. Y. Choe, C. Kang, S. I. Chang, M. H. Han, I. C. Kang, *Proteomics* **2006**, *6*, 1094.
[37] S. K. Kwak, G. S. Lee, D. J. Ahn, J. W. Choi, *Mater. Sci. Eng, C* **2004**, *24*, 151.
[38] J. Hyun, S. J. Ahn, W. K. Lee, A. Chilkoti, S. Zauscher, *Nano Lett.* **2002**, *2*, 1203.
[39] B. Sanii, A. N. Parikh, *Soft Matt.* **2007**, *3*, 974.
[40] J. Nissen, S. Gritsch, G. Wiegand, J. O. Radler, *Eur. Phys. J. B* **1999**, *10*, 335.
[41] J. Nissen, K. Jacobs, J. O. Radler, *Phys. Rev. Lett.* **2001**, *86*, 1904.
[42] D. Banerjee, N. A. Amro, S. Disawal, J. Fragala, *J. Microlith. Microfab.* **2005**, *4*, 230.
[43] P. Hoffmann, R. P. Mikalo, D. Schmeisser, *Solid-State Electron.* **2000**, *44*, 837.
[44] K. Salaita, A. Amarnath, D. Maspoch, T. B. Higgins, C. A. Mirkin, *J. Am. Chem. Soc.* **2005**, *127*, 11283.
[45] S. Lata, A. Reichel, R. Brock, R. Tampe, J. Piehler, *J. Am. Chem. Soc.* **2005**, *127*, 10205.
[46] J. T. Groves, N. Ulman, S. G. Boxer, *Science* **1997**, *275*, 651.
[47] E. A. Bayer, H. Benhur, M. Wilchek, *Methods Enzymol.* **1990**, *184*, 80.
[48] C. A. Helm, W. Knoll, J. N. Israelachvili, *Proc. Natl. Acad. Sci. USA* **1991**, *88*, 8169.
[49] C. Lou, Z. Wang, S. W. Wang, *Langmuir* **2007**, *23*, 9752.
[50] R. Reiter, H. Motschmann, W. Knoll, *Langmuir* **1993**, *9*, 2430.
[51] M. R. Horton, C. Reich, A. P. Gast, J. O. Radler, B. Nickel, *Langmuir* **2007**, *23*, 6263.
[52] M. Ahlers, W. Muller, A. Reichert, H. Ringsdorf, J. Venzmer, *Angew. Chem. Int. Ed.* **1990**, *29*, 1269.
[53] L. Schmitt, C. Dietrich, R. Tampe, *J. Am. Chem. Soc.* **1994**, *116*, 8485.
[54] I. T. Dorn, K. Pawlitschko, S. C. Pettinger, R. Tampe, *Biol. Chem.* **1998**, *379*, 1151.
[55] I. T. Dorn, K. R. Neumaier, R. Tampe, *J. Am. Chem. Soc.* **1998**, *120*, 2753.
[56] C. Dietrich, O. Boscheinen, K. D. Scharf, L. Schmitt, R. Tampe, *Biochemistry* **1996**, *35*, 1100.
[57] C. Dietrich, L. Schmitt, R. Tampe, *Proc. Natl. Acad. Sci. USA* **1995**, *92*, 9014.
[58] M. Chalfie, *Photochem. Photobiol.* **1995**, *62*, 651.
[59] I. Reviakine, A. Brisson, *Langmuir* **2001**, *17*, 8293.
[60] S. A. Darst, E. W. Kubalek, A. M. Edwards, R. D. Kornberg, *J. Mol. Biol.* **1991**, *221*, 347.
[61] I. Inoue, Y. Wakamoto, H. Moriguchi, K. Okano, K. Yasuda, *Lab Chip* **2001**, *1*, 50.
[62] T. Nakaji-Hirabayashi, K. Kato, Y. Arima, H. Iwata, *Biomaterials* **2007**, *28*, 3517.
[63] A. Thess, S. Hutschenreiter, M. Hofmann, R. Tampe, W. Baumeister, R. Guckenberger, *J. Biol. Chem.* **2002**, *277*, 36321.
[64] E. Soderlind, L. Strandberg, P. Jirholt, N. Kobayashi, V. Alexeiva, A. M. Aberg, A. Nilsson, B. Jansson, M. Ohlin, C. Wingren, L. Danielsson, R. Carlsson, C. A. K. Borrebaeck, *Nat. Biotechnol.* **2000**, *18*, 852.
[65] S. Lenhert, A. Sesma, M. Hirtz, L. F. Chi, H. Fuchs, H. P. Wiesmann, A. E. Osbourn, B. M. Moerschbacher, *Langmuir* **2007**, *23*, 10216.
[66] R. Parthasarathy, J. T. Groves, *Soft Matt.* **2007**, *3*, 24.
[67] C. Wingren, J. Ingvarsson, L. Dexlin, D. Szul, C. A. K. Borrebaeck, *Proteomics* **2007**, *7*, 3055.
[68] C. A. K. Borrebaeck, C. Wingren, *Expert Rev. Mol. Diagn.* **2007**, *7*, 673.

Received: July 4, 2008

